The Geological Map of Mimas v1.0-2023

Bradák, Balázs

Okumi, Motoharu

(Citation)
Geosciences,14(1):25

(Issue Date)
2024-01

(Resource Type)
journal article

(Version)
Version of Record

geosciences

MDPI

Article

The Geological Map of Mimas v1.0-2023

Balázs Bradák * and Motoharu Okumi

Laboratory of Exo-Oceans, Faculty of Oceanology, Kobe University, 5-1-1 Fukaeminami-Machi, Higashinada-ku, Kobe 658-0022, Japan

* Correspondence: bradak.b@port.kobe-u.ac.jp

Abstract: A theory about a young, evolving "stealth ocean" under the ancient-looking surface of Mimas, the moon of Saturn, triggered us to revisit the icy satellite and develop a revised geological map based on Cassini images. The re-mapping of Mimas's surface aimed to fill the decades-long gap that grew since the publication of the first Voyager image-based pioneering map, and it provided an up-to-date synthetic interpretation of revised and newly discovered features. Despite the map being in its early stage of introduction, it already showed some key features that may play significant roles in the reconstruction of Mimas's (surface) evolution. The Herschel crater, formed by a global-scale impact, undoubtedly left additional marks, including fault scarps, stair-step faults, and post-impact surface transformation, through mass movements around the crater wall and the peak. Smaller craters left various scars on the surface, including asymmetric craters, whose morphology and allocation we used to reconstruct the regional topographic changes on the surface of Mimas. In addition to the impact-related features, which dominated the surface of the icy satellite, groups of weak, quasi-parallel running linear features, such as undifferentiated lineaments, grooves/through, and ridges, were also observed. The appearance and pattern of those lineaments overlapped with the allocation of various modeled global nonlinear tidal dissipations, supporting the existence of theoretical subsurface stealth oceans.

Keywords: Mimas; Saturn; geological map; stealth ocean; tectonic evolution

Citation: Bradák, B.; Okumi, M. The Geological Map of Mimas v1.0-2023. *Geosciences* **2024**, *14*, 25. https://doi.org/10.3390/geosciences14010025

Academic Editors: Alberto G. Fairén and Jesus Martinez-Frias

Received: 25 December 2023
Revised: 15 January 2024
Accepted: 17 January 2024
Published: 22 January 2024

1. Introduction

Geological mapping is one of the most prolonged and fundamental methods in geological research. It is rooted in the studies of Martin Lister (1639–1712), a naturalist who suggested visualizing the soil type distribution on maps. Lister's idea was realized by Luigi Ferdinando Marsili (1658–1730). Following his contribution to the military by creating detailed maps of the landscape, including the rock outcrops, he mapped the distribution of gypsum and sulfur deposits around Bologna (1717), and later he published a map of mining districts in Hungary (1726) [1]. Unfortunately, the name of the cartographer who created the actual first geological map (1757) containing four different rock types, including sandstone (Bunter Sandstein, Buntsandstein), limestone (Mushelkalkstein), chalk (Kreide), and coal beds (Kohle), was lost. However, the three former rock types later became the basis of Mesozoic litho- and chronostratigraphy (Friedrich August von Alberti, 1834) [2].

Geological maps not only provide information about the geological features of a surface or the even areas below, but they also reveal the geological evolution of the studied area via the chronological and tectonic information embedded in the map.

In contrast to geological mapping on Earth, such expectations brought new challenges to researchers mapping the surfaces of various planetary bodies. Besides the Moon, geologists could not conduct fieldwork on different planetary bodies and draw geological maps based on their field observations.

Planetary mapping is divided into two significant periods: the phase of early observations from Earth (visual era), followed by the photographic era, which is when planetary

scientists based their mapping on photographs from various sources (spacecraft, orbiters, and so on) [3].

On-site automatic missions and later human missions to the Moon needed more accurate maps containing additional geological elements to determine landing sites. Such needs led to the geological and geomorphological mapping of specific areas on the surface of the Moon and the creation of the first photo-image-based "astrogeological" maps, which comprised surface morphologic–structural elements, various regions with surface materials with various characters, and the stratigraphic and consequently chronological relation of those elements [3]. Mapping these elements required the involvement of new fields concerned with the study of planetary bodies, such as geology and geomorphology. This resulted in the development of the multi- and interdisciplinary fields of planetology or planetary science. In recent decades, photo-image-based maps have been completed, with additional information provided by various sensors (e.g., laser and radar altimetry and reflectance spectroscopy), and paper maps and atlases have been replaced by GIS (geographical information system) databases, along with digitalized, renovated versions of old maps [3].

There has been considerable development in the geological mapping of the Moon and terrestrial planets, including Mercury, Mars, and even Venus, despite the difficulties caused by the planets' massive atmospheres. In contrast to those planetary bodies, the mapping of outer-solar-system objects, including the moons (also called satellites) of gas (Jupiter and Saturn) and ice giants (Neptune and Uranus), only started in the 1980s and was most likely triggered by two factors. There was a technical factor. Namely, the first spacecraft arrived at Jupiter (e.g., Voyager 1, 1979) and Saturn (e.g., Voyager 2, 1981) and sent the first images back to Earth around the end of the 1970s, allowing researchers to interpret various surface features and create the first maps of multiple satellites. An additional factor to be considered, which most likely triggered the renaissance of the study of outer-solar-system satellites, was the discovery of some subsurface water reservoirs and subsurface oceans on, e.g., Enceladus [4] and Europa [5,6], and the potential of life under the ice shell [7]. Along with the growing interest in the moons of the outer solar system, the list of potential icy satellites with subsurface oceans (harboring life) has been increasing exponentially [8,9].

Among the Jovian moons, Europa and Ganymede most likely have subsurface oceans hidden under their ice crusts [5,6,10–12]. The observed water plume on the images sent by Cassini's spacecraft provided evidence of a subsurface reservoir and/or ocean under the frozen surface of Enceladus, the moon of Saturn [4,13]. Along with Enceladus, one of the moons in the outer solar system that has the most potential regarding the existence of, e.g., microbial life, is Titan, which also hosts a subsurface liquid layer between two icy units in its interior [14]. Based on calculations in very recent studies, numerous satellites of Uranus, including Ariel, Umbriel, Titania, and Oberon, may host liquid spheres as subsurface oceans under their surfaces [15,16]. Like Uranus, one moon of Neptune, Triton, may hide an ocean under its ice shell [17].

Like Earth, oxidants must be transported downward from the icy surface to keep those subsurface oceans oxygenated and keep the potential biosphere alive [18]. Two mechanisms that may be capable of executing such transport and material exchange between the surface and subsurface regions are cryotectonism and cryovolcanism. Based on our current knowledge and given the existing resources, the easiest way to identify and characterize these processes is via remote sensing-based (e.g., image-based mosaic maps and photogrammetry) geological and geomorphological mapping of the target icy satellites.

The growing number of candidates with subsurface oceans and the importance of geological mapping in the understanding of surface processes and the evolution of icy moons (along with the reconstruction of the planetary environment and knowledge of possible exobiological evolution) have triggered the geological mapping of icy satellites, such as Europa [19], Ganymede [20] (Jupiter), Enceladus [21], Dione [22], Titan [23] (Saturn), and Triton [24] (Neptune) (Table 1).

Table 1. Comparison of the essential characteristics of ocean-bearing icy satellites with current global geological maps. Abbreviations: n—nighttime; d—daytime; m—mean; e—equator; p—pole; a—annual; min—minimum; max—maximum; geom. Albedo—geometric albedo (is the ratio of a body's brightness at zero phase angle to the brightness of a perfectly diffusing disk with the same position and apparent size as the body); ($a_{☾}$)—semi-major axis, compared to the Moon; AU—astronomical unit, which is the average distance of the Earth from Sun (approximately 150 million km); and $R_{⊕}$, $g_{⊕}$ and $p_{⊕}$—the radius, gravity and the atmospheric pressure of the satellites and the pressure of its atmosphere compared to the radius, gravity and atmospheric pressure of Earth, respectively. Along with the primary planetary data, gained from https://ssd.jpl.nasa.gov/sats/phys_par/ (accessed on 23 December 2023) and http://ssd.jpl.nasa.gov/?sat_phys_par#ref69 (accessed on 23 December 2023), additional information about the main characteristics used in this chart can be found in various studies such as [25,26] (Moon), [19,27–29] (Europa), [20,29–32] (Ganymede), [33–42] (Mimas), [21,33,34,43,44] (Enceladus), [22,33,34,45,46] (Dione), [23,47,48] (Titan), and [24] (Triton).

Satellite ($a_{☾}$)	$R_{⊕}$	$g_{⊕}$	T_{surf} (C°)	Surface Comp.; (geom. albedo)	Main Geological Features and Phenomena to Be Considered (Keywords)
Moon (1 $a_{☾}$)	0.27	0.17	−183 (n), 106 (d)	Lunar regolith: rock and mineral fragments, impact and volcanic glasses, and agglutinates (0.12)	Various impact craters, crater chains (catenae), mare and lacus regions (plains formed by extensive melting and extrusion of basaltic rock), mountains (remaining rims of giant impacts), rilles, and moonquakes. Exosphere (tenuous atm.): He, Ar, Na, K, CH_4, CO, CO_2, and O_2.
Europa (1.75 $a_{☾}$)	0.24	0.13	−143 (max), −177 (e), −227 (p), −183 (m)	H_2O ice, NaCl, colored areas: hydrated salts, SO_4^{2-}; (0.67)	Lineaments, ridges, troughs, bands, banded plains, chaos terrains, microfeatures, and impact craters; sporadic plums, cryovolcanism, subsumption, and active cryotectonism. Extremely tenuous atmosphere: O_2 and H_2O.
Ganymede (2.78 $a_{☾}$)	0.41	0.15	−183 to −113	H_2O ice, darkening agent; H_2SO_4 hydrate and salts (SO_4^{2-}, Cl^-), radiolytic processing; (0.43)	Old, highly cratered dark regions (~1/3 part of the surface) and bright grooved terrains, formed by tectonic and cryovolcanic processes (~2/3 part of the surface); cratered materials, basins, depressions, domes, palimpsest, furrows, and grooves. Tenuous, envelop atmosphere: O_2, O_3, and H_2O.
Mimas (0.48 $a_{☾}$)	0.03	0.01	≤−185 (d)	H_2O ice mainly (possibly from E ring), Appearance of NH_3 ?; (0.6)	Heavily cratered, Herschel impact and the global-scale impact-related tectonic features; stealth subsurface ocean. No detectable atmosphere.
Enceladus (0.62$a_{☾}$)	0.04	0.01	−185 to −163 (d),	Resurfacing by plume ices; H_2O, CO_2 ices, NH_3 and "tholins" (iron rich nanograins); (1.0)	Geologically active icy moon, intense tectonism, ridges, troughs, scarps (younger provinces), cratered terrains (older regions), cryovolcanism, and plume activity. Tenuous atmosphere (more significant than other icy moons, except Titan): H_2O, N_2, CO_2, CH_4, and traces of simple organic molecules.
Dione (0.98 $a_{☾}$)	0.09	0.02	−218 to −203 (n), −175 to −155 (d),	H_2O and CO_2 ices, NH_3, ferrous iron-bearing mineral, radiolytic processing; (0.6)	Heavily cratered regions, catenae, fossae, chasmata; putative active cryotectonism: rifting, faulting, and potential subsumption; cryovolcanism. Thin gas envelop (exosphere): O^{2+}, O_2, and O_3.
Titan (3.18 $a_{☾}$)	0.40	0.14	−179 to −180 (a)	H_2O, CH_4, NH_3 ices, hydrocarbons (in solid and liquid phase), rich in organic materials; (0.2)	Geological processes: impact cratering, pluvial, fluvial, and aeolian erosion and deposition, precipitation, dissolution, tectonism, and cryovolcanism. Thick, dense atmosphere: N_2 (~95%), CH_4 (~5%), and H_2 (<1%); 1.35–1.6 $p_{⊕}$.

Table 1. *Cont.*

Satellite (a꜀)	$R_{\oplus}$	$g_{\oplus}$	T_{surf} (C°)	Surface Comp.; (geom. albedo)	Main Geological Features and Phenomena to Be Considered (Keywords)
Triton (0.92 a꜀)	0.21	0.08	−235	H_2O, CH_4, CO, CO_2, HCN, and C_2H_6 ices; (0.76)	Very young surface, with various terrains: cantaloupe terrain(s), lineated terrains, etched plains, macular terrain, walled planitia, and bright lobate terrains; cavi and septa, ridges, scarps, knobs, depressions, mesa, paterae; plume activity, cryovolcanic features (smooth plains). Tenuous atmosphere: N_2, CH_4, and CO.

Despite numerous similarities, compared to most of the icy satellites listed in Table 1, Mimas has been considered an inactive moon, with no characteristic surface sign of global (cryo)tectonic activity and any significant, relatively young surface renewal processes. Based on the crater-counting method, the absolute age of the heavily cratered regions is around 4.3 Ga old, compared to the relatively young giant impact Herschel, which dates back roughly 4.1 Gyr ago [49].

Such common scientific knowledge about Mimas has been changing in the last decade, with a series of studies discussing the possibility of a subsurface "stealth" ocean below the frozen and ancient-looking surface of the satellite [36–42]. Although the appearance of a subsurface ocean looks plausible, there are still some controversies about the formation of a subsurface ocean and the lack of any characteristic marks of (cryo)tectonic processes on the surface, which may indicate indirectly the appearance of such a liquid layer below the ice crust. Based on various models, the lack of such surface features is explained in various ways, including a strong ice shell, which may withstand higher tidal stresses [39], or the young geological age of the subsurface ocean, which may explain the lack of tectonic features [42], i.e., the early tectonic evolution phase of the shell is "in progress" (e.g., even stagnant lid tectonism is still not recognizable [50]).

Along with the executed model studies, recognizing any surface mark of active or inactive stress fields feels crucial. This is not simply from the perspective of the existence of a subsurface ocean, which may harbor extraterrestrial life, but also for discerning the origin and evolution of the satellite itself. Observing potential marks of early-phase tectonism would support the theory about the "ring origin" of the moon instead of the primordial accretion theory [42]. Despite its time-consuming nature, global and detailed "fresh" Cassini image-based geological mapping of Mimas may solve some unanswered questions.

This study presents the first version of the semi-global geological map of Mimas, the icy satellite of Saturn, focusing on the first vital observations and raising concerns while interpreting the results.

2. Materials and Methods

During the global-scale geological mapping of the icy satellite, three base maps were used, namely Mimas Global Map—June 2017, Global 3-Color Map of Mimas (2014), and a supposedly earlier version of the former Mimas Global Map which appeared in the JMars version 5.3.15.2 (https://jmars.asu.edu/ (accessed on 23 December 2023)), named the Cassini ISS Cartographic Map of Mimas (Figure 1).

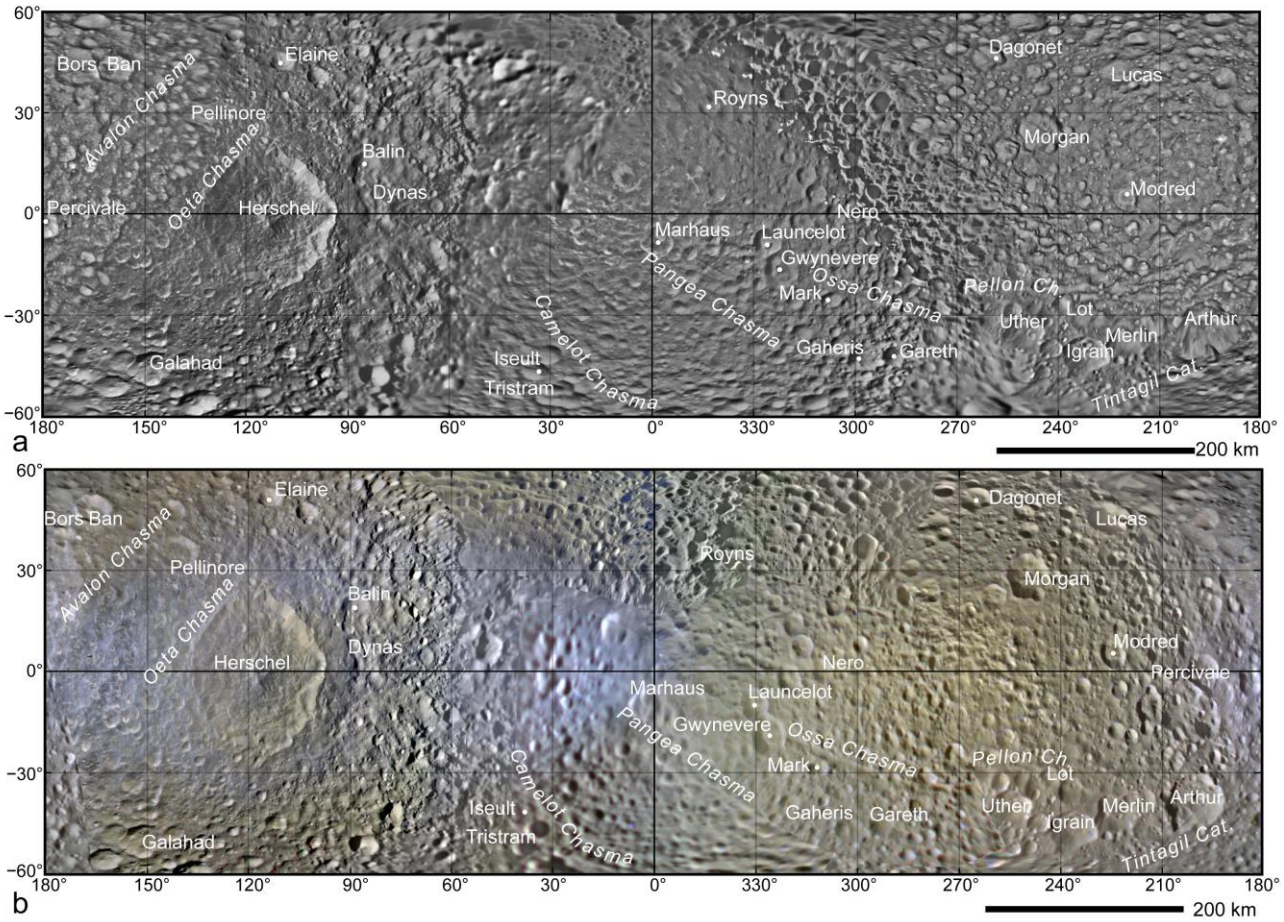

Figure 1. A cutout of the studied area from the "Mimas Global Map" was used during the geological mapping. Map (**a**) is a cutout from Mimas Global Map—June 2017 version, published on the site of NASA Jet Propulsion Laboratory, California Institute of Technology (https://www.jpl.nasa.gov/images/pia17214-mimas-global-map-june-2017 (accessed on 23 December 2023)). Map (**b**) is a cutout from Global 3-Color Map of Mimas (2014), published on the site of NASA Jet Propulsion Laboratory, California Institute of Technology (https://www.jpl.nasa.gov/images/pia18437-color-maps-of-mimas-2014 (accessed on 23 December 2023)). The present study analyzed no regions beyond a latitude +/−60° because of the projection system-triggered distortion around the polar regions. The applied nomenclature follows the recommendation of the Gazetteer of Planetary Nomenclature (https://planetarynames.wr.usgs.gov/Page/MIMAS/target (accessed on 23 December 2023)). Colors in the global mosaics of the Global 3-Color Map of Mimas are enhanced false colors.

Despite the similarity between the former (Mimas Global Map—June 2017) and the Cassini ISS Cartographic Map, there are significant differences between the two image mosaic maps. Such differences were found during the mapping, e.g., in the shape of craters, and are discussed in Sections 3 and 4. Both maps are mainly based on images taken during Cassini spacecraft flybys during the cooperative Cassini–Huygens mission between NASA, the European Space Agency, and the Italian Space Agency. While creating the Cassini ISS Cartographic Map of Mimas, Voyager 1 and 2 images were also used to fill some gaps. Compared to the mosaic that appears in Jmars, which looked very similar to the published initially Mimas global mosaic map, called Map of Mimas—June 2012 (https://photojournal.jpl.nasa.gov/catalog/PIA14926 (accessed on 23 December 2023)), the suggested 2012 version was updated with new images following the two most recent flybys in November 2016 and February 2017, and published as Map of Mimas—June 2017 (https://www.jpl.nasa.gov/images/pia17214-mimas-global-map-june-2017 (accessed on 23 December 2023)).

Along with the two versions of Cassini image mosaic maps, the Color Map of Mimas—2014 (https://www.jpl.nasa.gov/images/pia18437-color-maps-of-mimas-2014 (accessed on 23 December 2023)) was also used as a reference during the study. The image selection, radiometric calibration, geographic registration, and photometric correction, as well as mosaic selection and assembly, were performed at the Lunar and Planetary Institute (Houston, TX, USA).

The suggested update (June 2017) changed some of the map's content, which potentially affected the interpretation of certain features. It resulted in the use and comparison of the three maps listed above during the geological mapping. The bias triggered by the differences between the maps is discussed in a later section of the study.

Along with the Cassini image-based global mosaic maps, maps and descriptions from the earliest publications about Mimas geology were also used [51,52].

The applied nomenclature followed the recommendation of the Gazetteer of Planetary Nomenclature (https://planetarynames.wr.usgs.gov/Page/MIMAS/target (accessed on 23 December 2023)).

Geological mapping and some related GIS research were performed using QGIS 3.22 software, followed by statistical analysis, which was executed with various Python 3.10.4 software packages, including NumPy 1.22.012, matplotlib, pandas, SciPy 1.8.0, and seaborn. All features, craters, and structural elements were interpreted visually and digitized interactively from the high-resolution and georeferenced images in QGIS 3.22. Basic information about the craters and lineaments was collected in a QGIS database and was used as a primary source for the analysis in Python 3.10.4 software. Besides the two basic geological maps published in the early 1990s [51,52], no datasets were used during the geological mapping. All presented results are connected to the executed research; no other database was used.

Considering the goal of this study, i.e., introducing the preliminary results of the mapping, the study does not contain the results of the in-progress stratigraphic (morphostratigraphy) and chronologic analysis to avoid jumping to too-early conclusions about Mimas' surface evolution.

3. Results

3.1. Impact Craters

During the identification of impact structures on the surface of Mimas, more than four thousand (4048) craters were found. Impact craters belonging to the simple crater main category were the most common structures (90.9%; Figure 2a).

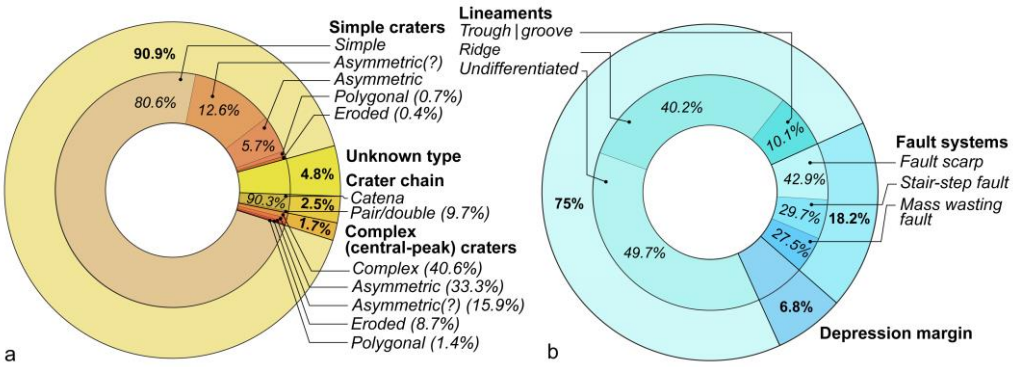

Figure 2. Donut charts indicate the ratio of the main (outer ring) and subcategories (inner circle) of craters (**a**) and various tectonic features (**b**). Bold letters and values indicate the main categories, and their ratio considers all the other main categories. Cursive letters and values indicate the types of subcategories and their percentage. considering the other subcategories under the same primary category. "?" shows the barely identifiable and potentially distorted craters, defined as putative asymmetric craters (please find more information in Section 4.1).

Despite the basic morphological similarities between the impact craters belonging to the main category of simple crater, some key differences existed between the identified subcategories. Simple craters belonged to the subcategory named as the primary category itself, characterized by a geometrically simple, bowl-shape structure with some lens-shape accumulation of the debris following the collapse of the rim (80.6%; Figures 2a and 3) [53–55].

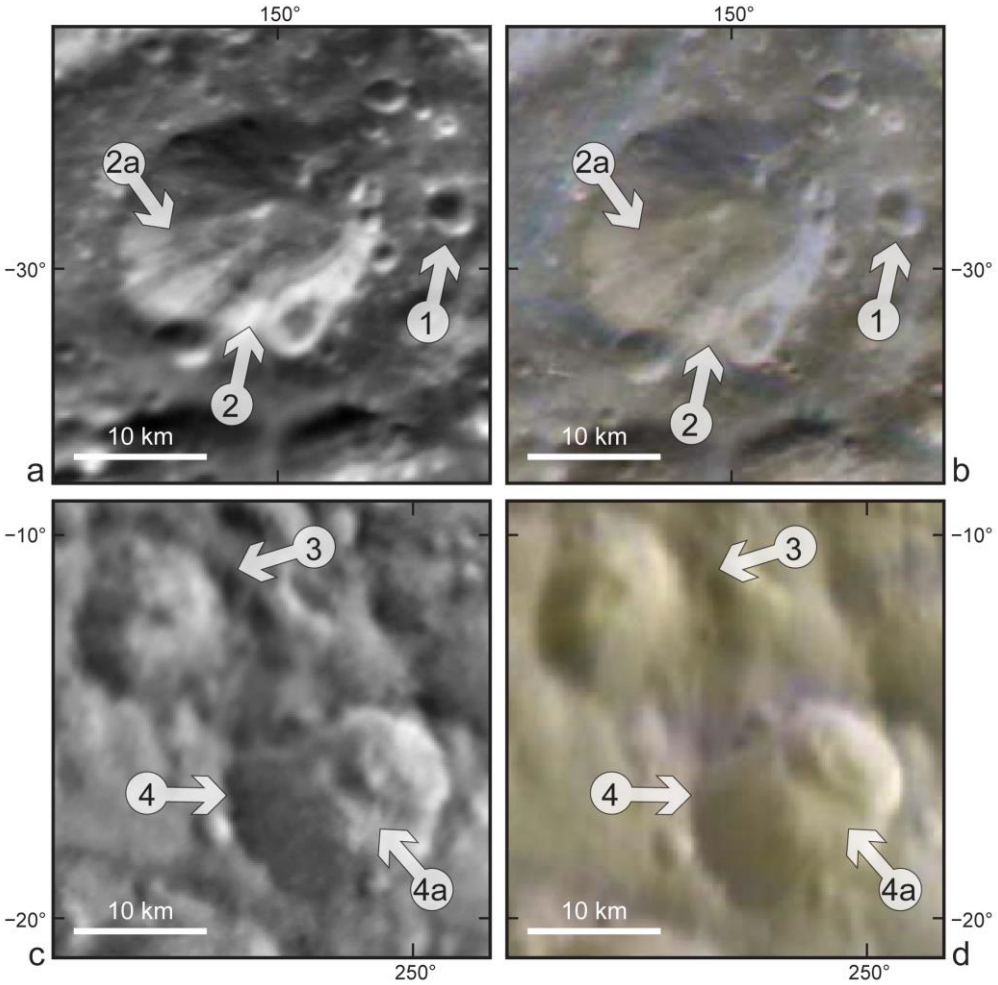

Figure 3. Some of the most common impact craters cover the surface of Mimas. The pairs of images a and b, and c and d show the differences between the 2012/2017 Mimas global mosaic map (**a**,**c**) and the Global 3-Color Map of Mimas (**b**,**d**). The markers with numbers show the same craters appearing in various mosaics. 1—simple crater; 2—asymmetric crater with lens-shape accumulation in the crater floor and layer-like structures indicated by various albedo, exposed in the crater wall (2a); 3—complex (central-peak) crater; and 4—asymmetric crater with a central-peak-like structure and a terrace-like feature, or a toe of a mass wasting, reforming the crater wall (4a).

Asymmetric simple impact craters (including the ones that are barely recognizable or questionable because of distortion appeared, e.g., during image processing and were defined as putative asymmetric craters, marked by "?") seem to be relatively common on the surface of Mimas (12.6 and 5.7%; Figures 2a and 3). Their asymmetric elliptical shape and irregular morphology may indicate oblique impacts [56–58], impact-related surface degradation around the neighborhood of the crater (e.g., ricocheting projectiles) [58], and impact on the slope [59].

Despite their importance in indicating possible endogenic (tectonic) and exogenic (surface erosion) processes [60,61], the ratio of identified polygonal (0.7%; Figure 2a) and eroded craters (0.4%; Figure 2a) is small compared to the other two simple and asymmetric crater types.

The mean minimum diameter ($Ø_{MIN}$) of simple craters spans between 3 and 13 km, with areas ranging from a minimum of 1 to a maximum of 1515 km^2. Among the various subcategories, polygonal simple craters are significantly more extensive than the other types (a_{MEAN}: 255 km^2, a_{MIN}: 5 km^2, a_{MAX}: 1515 km).

Compared to the simple craters, significantly fewer complex craters, specified by their characteristic central peak [55], were found on the surface of Mimas (1.7%; Figure 2a). This type of subcategories belongs to complex craters, and their ratio is like that of simple craters. Among the main category of complex crater, most of the craters belong to the complex crater subcategory (40.6%; Figure 2a), characterized by a broad, often flat, and shallow crater floor, wall-terrace structures, and most importantly, a central peak raised during the formation of the impact crater. The ratio of asymmetric (33.3%) and putative asymmetric craters (15.9%) together reached the number of complex craters. Significantly fewer numbers eroded (8.7%), and only one polygonal complex impact crater (Herschel) was found on the surface of Mimas (Figure 2a).

The mean $Ø_{MIN}$ of complex craters was significantly more extensive than the impact craters of other main categories, falling between 13 and 16 km, together with an extreme member, Herschel, characterized by $Ø_{MIN}$: ~130 km.

Of the 4048 impact craters, 196 (4.8%, Figure 2a) were classified as "unknown" crater types. This main category comprised putative impact craters, most likely belonging to one of the primary categories or subcategories introduced above. Still, the quality/resolution of certain parts of the image mosaic map made it impossible to provide further information and elaborate classification.

Along with the two main crater categories and the additional "unknown" group, craters belonging to impact crater chains were mapped separately. Based on morphological differences, impact crater chains were separated into two subcategories: impact crater pairs (or doubles, consisting of two craters) and catena (or crater chain) [62]. The size of both subcategories was very similar, $Ø_{MIN}$: 3 and 4 km, respectively. The size of the members of the crater chains seemed slightly smaller than that of craters that belonged to the other main categories.

3.2. Potential Tectonic Features

During the geological mapping of the moon's surface, five hundred (501) quasi-linear features were identified and classified into three main and seven subcategories (Figure 2b).

Features belonging to the main category of lineaments were the most dominant on the moon's surface (75%; Figure 2b). It comprises three subcategories: undifferentiated lineaments, troughs, and ridges. Among the three subcategories, undifferentiated lineaments are the most common (49.7%), followed by ridges (40.2%) and troughs (10.1%) (Figures 2b and 4a–d). Instead of appearing as individual features, most of them run together as quasi-parallel, sometimes curvy, groups of lineaments at various locations on the icy surface of Mimas. Such a group of quasi-parallel lineaments was all together interpreted as chasmata (a deep, elongated, steep-sided depression [63]), such as Ossa and Pangea Chasma, in an earlier report [52] based on lower-resolution images.

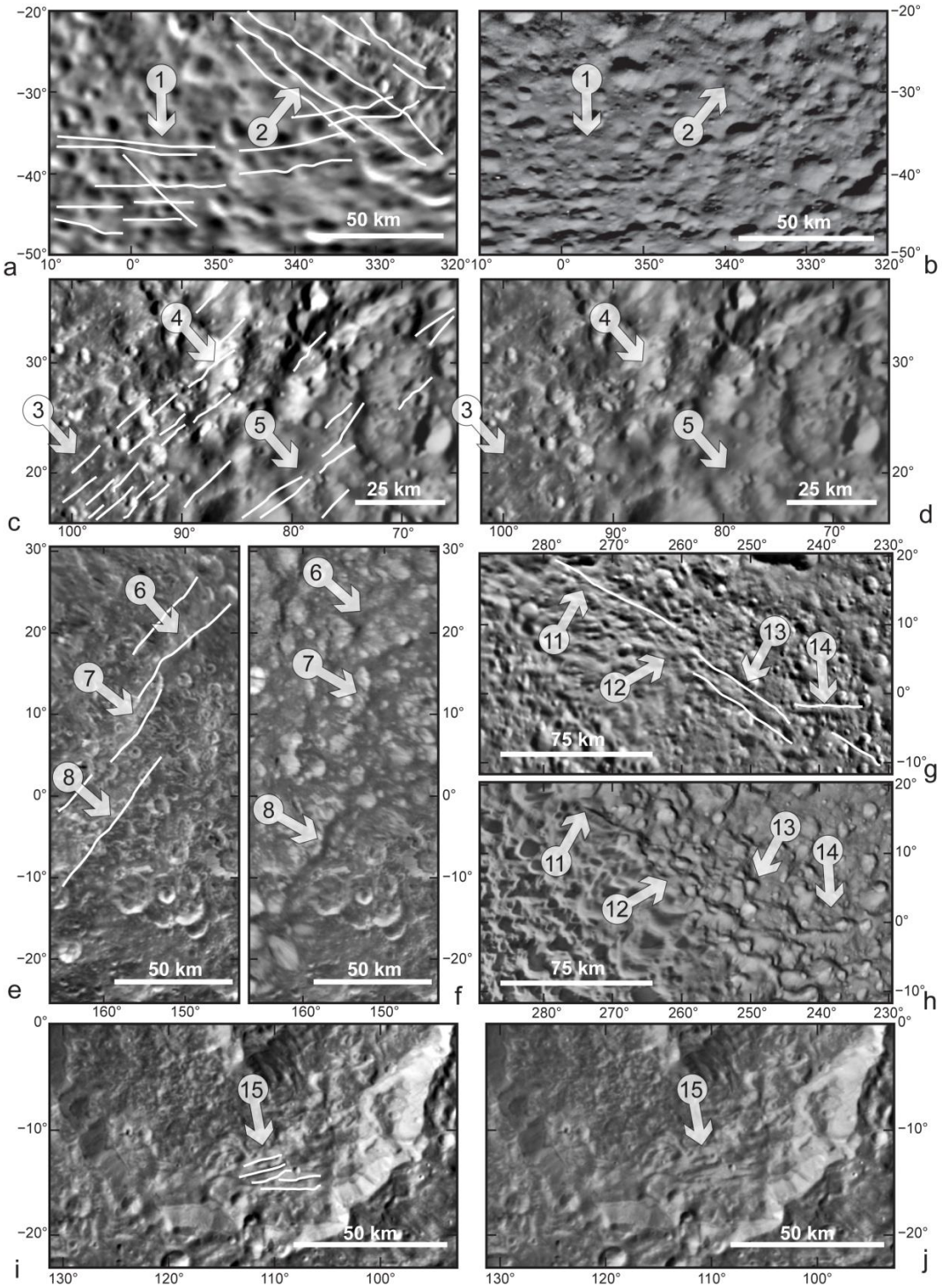

Figure 4. Main types of putative tectonic features identified on the surface of Mimas. The group of images (**a**–**j**) shows the differences between the 2012 and 2017 Mimas global mosaic map (please find a detailed explanation in Section 2). The markers with numbers pinpoint the same putative tectonic features appearing in various versions of the image mosaic maps. 1—curved structure of quasi-parallel trough (grooves) and ridges; 2—ridge; 3–5—quasi-parallel set of undifferentiated lineaments, mainly visible because of the albedo differences between the lineaments (narrow, brighter features) and the surrounding environment; 6–8—fault scarps (or interpreted together: stair-step faults); 11–14—(pseudo-) stair-step faults (detailed explanation can be found in Sections 3.2 and 4.2); 15—mass movement scarp.

The most common fault-scarps (42.9%), stair-step faults (29.7%), and mass movements scarps (27.5%) were the three subcategories within the main category of fault systems (18.2%) (Figure 4e–j). The subcategories fault scarps and stair-step fault comprised features whose morphology pointed toward some alternative theory regarding their origin (Figure 4g,h). Based on the earlier (2012) version of the image mosaic map, the questionable features were likely defined as fault-scarps and stair-step faults (features 11 to 14; Figure 4g). The updated image mosaic map shows slightly different structures with different morphology, suggesting the role of impact craters in forming the fault-scarp/stair-step fault-like "pseudo" features (a detailed discussion can be found in Section 4.2). An earlier report interpreted one group of fault-scarps and stair-step faults as Avalon Chasma [52].

The third main category comprises features formed by mass movements. Despite the relatively high ratio compared to other main types (27.5%; Figure 2b), the allocation of mass movement scarps is concentrated around the Herschel impact crater (Figures 4i,j and 5). Similar features may appear around complex impact craters, but, unfortunately, the resolution of the image mosaics is most likely too low to identify smaller-scale mass movements.

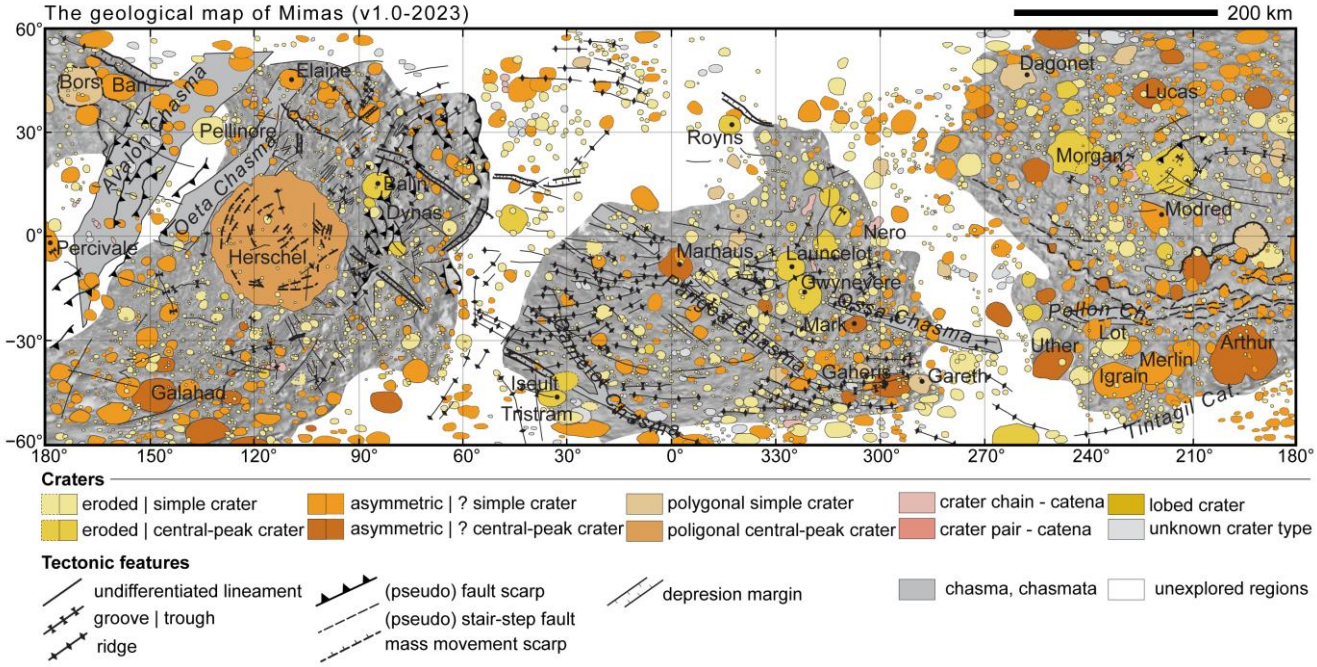

Figure 5. The first version of the revised geological map of Mimas (v1.0-2023).

4. Discussion—The Geological Map of Mimas (v1.0-2023)

4.1. Impact Crater Types and Their Potential in the Reconstruction of Geological Processes

As summarized above (Section 3.1) and shown in the geological map (Figure 5), numerous types of craters have been identified on the surface of Mimas. Various main categories and subcategories have different potential in terms of reconstructing the planetary environment and the evolution of the icy satellite's surface. In the following, such potential will be summarized without going into detail but pointing toward future research topics related to the moon.

(i) Simple and complex craters. The morphological differences between simple and complex (central peak) craters were among the earliest research topics on impact crater formation [53–55]. Beyond crater chronology and determination of the surface age [49], the size of the craters may allow further research, targeting surface renewal processes by various energy impacts, their ricocheting ejectiles, and finer grain ejecta blankets [58,64].

(ii) Asymmetric craters. Asymmetric craters are known as indicators of oblique asteroid impacts when the impact angle is relatively low (<45°, ~10–20°), which results in the formation of elliptical, asymmetrical-shaped craters [56–58]. Besides oblique impacts, the

mapping and interpretation of the orientation and allocation of certain asymmetric crater types on Vesta revealed the topographic control over their formation and their potential in the reconstruction of slopes [59]. Unfortunately, the characterization of asymmetric crater orientation and distribution is complex in Mimas's case.

As shown in the study about Vesta [59], the crater morphology plays a crucial role in describing the slope characteristics. In the case of Mimas, the morphology-based crater and slope classification seems complicated because of the changing appearance of the craters in various versions and mosaic parts of the used Mimas maps (Figure 6). The possible differences may relate to multiple image processing steps during the process of updating the 2012 mosaic map with the new images, which arrived in 2016–2017 (please see the Data and Methods section for more information). Although there is great potential in analyzing the asymmetric craters with regard to the characterization of regional-scale topographic features on the surface of Mimas, as a first step, a thorough filtering of the questionable craters is necessary to avoid biasing the results in the upcoming studies.

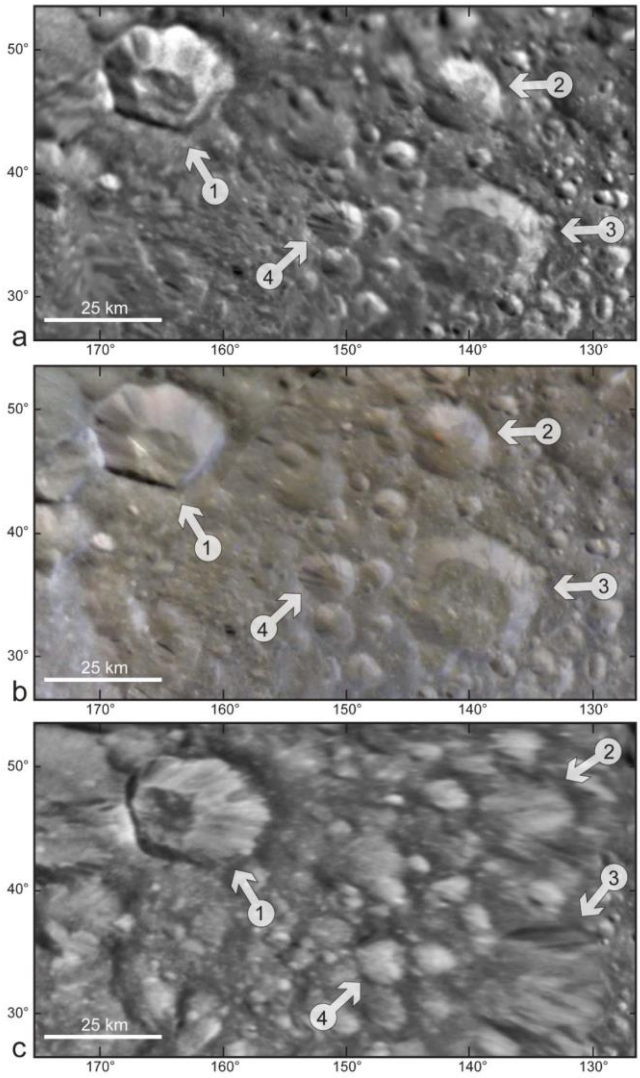

Figure 6. Various image mosaic maps exhibit differences in asymmetric crater morphology. Some of the most common impact craters cover the surface of Mimas. (**a**,**c**) The differences between the 2012 and 2017 versions of the Mimas global mosaic map and (**b**) the Global 3-Color Map of Mimas. The markers with numbers show the same craters appearing in various mosaics. The orientation in the asymmetric craters is recognizable, and regardless of their origin, such differences may bias the interpretation of asymmetric crater types in reconstructing sloping surfaces.

(iii) Polygonal craters. Despite their relatively low number on the surface of Mimas, polygonal craters may indicate endogenic processes, hidden or barely visible tectonic features, and various stress fields appearing in different planetary bodies, including the icy crust of the satellites of gas and ice giants. Craters can be defined as polygonal craters if they have one straight rim segment. Such a morphology may be formed by normal and strike-slip faults and lithological boundaries [61,65–67]. It is essential to mention that the relatively low ratio of polygonal craters (along with the eroded craters) may be biased by the quality of image mosaics (e.g., low-resolution), which prevents the clear identification of the markers of such crater types. Despite the suggested difficulties, the accurate mapping of polygonal craters and the study of their distribution may reveal hidden tectonic features related to the evolution of the stealth ocean and the icy crust of Mimas.

(iv) Eroded craters. Similar to polygonal craters, only a few eroded craters have been identified on the surface of Mimas (Figures 2b and 4). A degraded structure marks eroded craters compared to their pristine state. Such a degraded form is indicated by removing the crater-forming material and destroying the crater rim, resulting in discontinuous morphology or a structure with minimal or no relief compared to the surrounding terrain [60]. Eroded craters may imply exogenic and endogenic processes and provide additional information about the evolution of the icy surface.

(v) Crater chains. Crater chains (along with double/pair and multiple craters) occur on various planetary bodies. They are known to be the result of the impact of broken-up projectiles of a weak asteroid or comet [68]. Besides the broken-up projectiles, chain craters may form due to the impact of binary asteroids or comets (crater pairs or double craters) [62], and materials ejected by a giant impact can appear on another satellite [69].

4.2. The Distribution of Putative Tectonic Features and Their Origin

Earlier studies [39] suggested that Mimas ice shell may be strong enough to withstand higher tidal stress than Europa's, referring to the lack of tectonic features. Along with the early studies published about the geology of Mimas [51,52], the introduced Cassini image-based geological map (Figure 5) indicates a slightly different situation. The identified tectonic features are far less characteristic than the icy moons with the marks of apparent tectonic activity (Table 1). Still, the distribution and pattern of simple features may help to identify the processes related to the Herschel-crater-forming impact and post-impact evolution of the surface, along with possible putative tectonic processes connected to an evolving subsurface ocean.

The existence of the Herschel crater, the mark of a global scale impact, implies the impact origin of at least some features [70,71]. Specific landforms and tectonic features may connect the seismic wave of the impact, the antipodal effect, or the formation of concentrical rings around the impact [71]. The pattern of Avalon Chasma and its newly recognized section running "around" the Modred impact crater on Mimas (stair-step faults; Figures 4g,h and 5) [51] is like the pattern of Ithaca Chasma, possibly related to the Odysseus-forming impact on the surface of Tethys. The formation of the identified fault scarps and stair-step fault system may be an analog to Ithaca Chasma, and its appearance can be explained by the whole-body oscillation of Mimas triggered by the impact [72]. The development of such tectonic features might be part of forming a ring-graben structure during the impact event, triggered by the collapse of the crater floor, involving materials from the moon's interior [73]. Regarding the formation of a disrupted antipodal terrain at the opposite of the Herschel impact, no clear geological marks can be observed, in agreement with some simulations, which indicates that the peak tensile stress does not exceed the rapture strength that may cause the fracturing of the surface [70].

Identifying the Ithaca Chasma-like regional-to-global-level feature in the ice crust of Mimas may support the tectonic origin of the fault-scarp/stair-step fault system placed in the neighborhood of the Modred impact crater (Figure 4g). Still, its tectonic origin was questioned after analyzing the updated image mosaic map (Figure 4h). The connection

between the questioned feature and the fault-scarp system of Avalon Chasma can be easily recognized by the analysis of the geological map (Figure 5).

As an alternative to impact origin, the globally appearing parallel and concentric pattern of simple lineaments such as undifferentiated lineaments, ridges, and troughs may indicate the influence of an evolving stealth ocean and tidal forces occurring in the ice crust (Figure 5) [39,40,42]. Compared to the surface of icy satellites with evident marks of tectonic processes (e.g., Europa, Ganymede, Enceladus, and Dione; Table 1), the lineament on the surface of Mimas is barely recognizable, and no complex features can be identified on the heavily cratered surface of the moon (Figures 4 and 5). As suggested above, Mimas was considered a tectonically inactive, "relict" satellite for a long time until the theory of a subsurface stealth ocean appeared [36–42]. Modeling an internal structure with the existence of a subsurface ocean suggested that, at the time of the Herschel-forming impact, the ice crust had to be thicker ($\geq$55 km) than the thickness of present-day ice shell hiding an ocean below it (<30 km) [41]. This conclusion leads to a theory that suggests that the ice shell of Mimas has been getting thinner, at least since the formation of the Herschel crater, and may imply a ring origin of Mimas, favored over the primordial accretion in the circum-planetary disk around the gas giant [42].

A thinning crust and a young, evolving subsurface ocean would explain the lack of complex tectonic features (e.g., various bands on Europa and Ganymede, [29]). As suggested by Prockter and Patterson [74], simple linear features (e.g., cracks and ridges) may evolve more and more complex structures (e.g., ridged bands) during the evolution of Europa's surface. As an analog to Europa, undifferentiated lineaments, ridges, and troughs may represent a juvenile, early tectonic evolution phase on the ice shell of Mimas.

The appearance of quasi-parallel trough-ridge structures may indicate the thinning of the crust [29] and periodic dilatation–compression cycles ("tidal squeezing") [75] and points toward the development of more complex, band-like structures [29,74]. Comparing the pattern of some of the lineament groups with some of the simulated patterns of tidal heating, the allocation of the lineaments on Mimas' surface may overlap with the modeled global nonlinear tidal dissipation in the putative subsurface ocean [76–78].

5. Conclusions

Introducing the first version of the revised Mimas geological map revealed the potential of asymmetric craters in the topography reconstruction and related flaws during the mapping process. Along with such defects, the preliminary results showed the existence of a supposedly young lineament network. The pattern of the lineament network may be formed by tidal forces related to stress fields in the ice shell, implying an evolving subsurface ocean. Along with providing indirect evidence of the subsurface ocean, the appearance of overlapping lineament generations promises a more detailed, morphostratigraphy-based chronological analysis of the surface evolution in subsequent studies.

As a preliminary study, the first version of the revised geological map of Mimas has flaws and numerous tasks to address in the following research step. Beyond the report and brainstorming-like introduction of various phenomena on the satellite's surface, a detailed explanation of multiple futures and their role in reconstructing the moon's geological history is necessary. From the angle of historical geology (planetary history), the detailed morpho- and chronostratigraphic study of the identified features is essential. Executing those steps in geological mapping may help to answer the critical question about the existence and evolution of a stealth ocean hiding below the icy crust of Mimas.

Author Contributions: Conceptualization, B.B.; methodology, B.B.; formal analysis, B.B. and M.O.; writing—original draft preparation, B.B. and M.O.; visualisation, B.B. and M.O. All authors have read and agreed to the published version of the manuscript.

Funding: This research received no external funding.

Data Availability Statement: Data related to this research will be sent upon request.

Acknowledgments: We want to thank the reviewers of this article for taking the time and effort to review the manuscript. We appreciate their valuable comments and suggestions, which helped improve this manuscript's quality.

Conflicts of Interest: The authors declare no conflicts of interest.

References

1. Franceschelli, C.; Marabini, S. Luigi Ferdinando Marsili (1658–1730): A pioneer in geomorphological and archaeological surveying. In *The Origins of Geology in Italy*; Geological Society of America (GSA) Special Papers, USA; Battista Vai, G., Glen, W., Caldwell, E., Eds.; Geological Society of America: Boulder, CO, USA, 2006; Volume 411. [CrossRef]
2. Oldroyd, D. Maps as pictures or diagrams: The early development of geological maps. In *Rethinking the Fabric of Geology*; Geological Society of America (GSA) Special Papers, USA; Baker, V.R., Ed.; Geological Society of America: Boulder, CO, USA, 2013; Volume 502. [CrossRef]
3. Hargitai, H.; Naß, A. Planetary Mapping: A Historical Overview. In *Planetary Cartography and GIS. Lecture Notes in Geoinformation and Cartography*; Hargitai, H., Ed.; Springer: Cham, Switzerland, 2019. [CrossRef]
4. Hansen, C.J.; Esposito, L.; Stewart, A.I.F.; Colwell, J.; Hendrix, A.; Pryor, W.; Shemansky, D.; West, R. Enceladus' water vapor plume. *Science* **2006**, *311*, 1422–1425. [CrossRef] [PubMed]
5. Sparks, W.B.; Hand, K.P.; McGrath, M.A.; Bergeron, E.; Cracraft, M.; Deustua, S.E. Probing for evidence of plumes on Europa with HST/STIS. *Astrophys. J.* **2016**, *829*, 121. [CrossRef]
6. Paganini, L.; Villanueva, G.L.; Roth, L.; Mandell, A.M.; Hurford, T.A.; Retherford, K.D.; Mumma, M.J. A measurement of water vapor amid a largely quiescent environment on Europa. *Nat. Astron.* **2020**, *4*, 266–272. [CrossRef]
7. Hansen, C.J.; Esposito, L.W.; Colwell, J.E.; Hendrix, A.R.; Portyankina, G.; Stewart, A.I.F.; West, R.A. The composition and structure of Enceladus' plume from the complete set of Cassini UVIS occultation observations. *Icarus* **2020**, *344*, 113461. [CrossRef]
8. Hussmann, H.; Sotin, C.; Lunine, J.I. Interiors and Evolution of Icy Satellites. *Treatise Geophys.* **2007**, *10*, 509–539. [CrossRef]
9. Nimmo, F.; Pappalardo, R.T. Ocean worlds in the outer solar system. *J. Geophys. Res. Planets* **2016**, *121*, 1378–1399. [CrossRef]
10. Carr, M.; Belton, M.; Chapman, C.R.; Davies, M.E.; Geissler, P.; Greenberg, R.; McEwen, A.S.; Tufts, B.R.; Greeley, R.; Sullivan, R.; et al. Evidence for a subsurface ocean on Europa. *Nature* **1998**, *391*, 363–365. [CrossRef]
11. Kivelson, M.G.; Khurana, K.K.; Russel, C.T.; Volwerk, M.; Walker, R.Y.; Zimmer, C. Galileo magnetometer measurements: A strong case for the subsurface ocean at Europa. *Science* **2000**, *289*, 1340–1343. [CrossRef]
12. Saur, J.; Duling, S.; Roth, L.; Jia, X.; Strobel, D.F.; Feldman, P.D.; Christensen, U.R.; Retherford, K.D.; McGrath, M.A.; Musacchio, F.; et al. The search for a subsurface ocean in Ganymede with Hubble Space Telescope observations of its auroral ovals. *J. Geophys. Res. Space Phys.* **2015**, *120*, 1715–1737. [CrossRef]
13. Porco, C.C.; Helfenstein, P.; Thomas, P.C.; Ingersoll, A.P.; Wisdom, J.; West, R.; Neukum, G.; Denk, T.; Wagner, R.; Roatsch, T.; et al. Cassini observes the active south pole of Enceladus. *Science* **2006**, *311*, 1393–1401. [CrossRef]
14. Vincent, D.; Lambrechts, J.; Tyler, R.H.; Karatekin, Ö.; Dehant, V.; Deleersnijder, É. A numerical study of the liquid motion in Titan's subsurface ocean. *Icarus* **2022**, *388*, 115219. [CrossRef]
15. Bierson, C.; Nimmo, F. A note on the possibility of subsurface oceans on the Uranian satellites. *Icarus* **2022**, *373*, 114776. [CrossRef]
16. Castillo-Rogez, J.; Weiss, B.; Beddingfield, C.; Biersteker, J.; Cartwright, R.; Goode, A.; Melwani Daswani, M.; Neveu, M. Compositions and interior structures of the large moons of Uranus and implications for future spacecraft observations. *J. Geophys. Res. Planets* **2023**, *128*, e2022JE007432. [CrossRef] [PubMed]
17. Hansen, C.J.; Castillo-Rogez, J.; Grundy, W.; Hofgartner, J.D.; Martin, E.S.; Mitchell, K.; Nimmo, F.; Nordheim, T.A.; Paty, C.; Quick, L.C.; et al. Triton: Fascinating Moon, Likely Ocean World, Compelling Destination! *Planet Sci. J.* **2021**, *2*, 137. [CrossRef]
18. Howell, S.M.; Pappalardo, R.T. NASA's Europa Clipper—A mission to a potentially habitable ocean world. *Nat. Commun.* **2020**, *11*, 1311. [CrossRef] [PubMed]
19. Leonard, E.J.; Patthoff, A.; Senske, D.A. Geological mapping of Europa at global and regional scales. In *Planetary Geologic Mappers 2019*; USGS Astrogeology Science Center: Flagstaff, AZ, USA, 2019; LPI Contrib. No. 2154, 12–14 June 2019, 7032.pdf; Available online: https://www.hou.usra.edu/meetings/pgm2019/pdf/7032.pdf (accessed on 17 November 2023).
20. Collins, G.C.; Patterson, G.W.; Head, J.W.; Pappalardo, R.T.; Prockter, L.M.; Lucchitta, B.K.; Kay, J.P. *Global Geologic Map of Ganymede*; U.S. Geological Survey: Reston, VA, USA, 2013. [CrossRef]
21. Crow-Willard, E.N.; Pappalardo, R.T. Structural mapping of Enceladus and implications for formation of tectonized regions. *J. Geophys. Res. Planets* **2015**, *120*, 928–950. [CrossRef]
22. Stephan, K.; Jaumann, R.; Wagner, R.; Clark, R.N.; Cruikshank, D.P.; Hibbitts, C.A.; Roatsch, T.; Hoffmann, H.; Brown, R.H.; Filiacchione, G.; et al. Dione's spectral and geological properties. *Icarus* **2010**, *206*, 631–652. [CrossRef]
23. Lopes, R.M.C.; Malaska, M.J.; Schoenfeld, A.M.; Solomonidou, A.; Birch, S.P.D.; Florence, M.; Hayes, A.G.; Williams, D.A.; Radebaugh, J.; Verlander, T.; et al. A global geomorphologic map of Saturn's moon Titan. *Nat. Astron.* **2020**, *4*, 228–233. [CrossRef]
24. Schenk, P.M.; Beddingfield, C.B.; Bertrand, T.; Bierson, C.; Beyer, R.; Bray, V.J.; Cruikshank, D.; Grundy, W.M.; Hansen, C.; Hofgartner, J.; et al. Triton: Topography and geology of a probable ocean world with comparison to Pluto and Charon. *Remote Sens.* **2021**, *13*, 3476. [CrossRef]

25. Jaumann, R.; Hiesinger, H.; Anand, M.; Crawford, I.A.; Wagner, R.; Sohl, F.; Jolliff, B.L.; Scholten, F.; Knapmeyer, M.; Hoffmann, H.; et al. Geology, geochemistry, and geophysics of the Moon: Status of current understanding. *Planet. Space Sci.* **2012**, *74*, 15–41. [CrossRef]
26. Kramer, G. Origin, Geography, and Geology of the Moon. In *Handbook of Lunar Base Design and Development*; Eckart, P., Aldrin, A., Eds.; Springer: Cham, Switzerland, 2020. [CrossRef]
27. Ashkenazy, Y. The surface temperature of Europa. *Heliyon* **2019**, *5*, e01908. [CrossRef]
28. Greenberg, R.; Geissler, P.; Hoppa, G.; Tufts, B.R. Tidal-tectonic processes and their implications for the character of Europa's icy crust. *Rev. Geophys.* **2002**, *40*, 1004. [CrossRef]
29. Howell, S.M.; Pappalardo, R.T. Band formation and ocean-surface interaction on Europa and Ganymede. *Geophys. Res. Lett.* **2018**, *45*, 4701–4709. [CrossRef]
30. Ligier, N.; Paranicas, C.; Carter, J.; Poulet, F.; Calvin, W.M.; Nordheim, T.A.; Snodgrass, C.; Ferellec, L. Surface composition and properties of Ganymede: Updates from ground-based observations with the near-infrared imaging spectrometer SINFONI/VLT/ESO. *Icarus* **2019**, *333*, 496–515. [CrossRef]
31. Squyres, S.W. Surface temperatures and retention of H_2O frost on Ganymede and Callisto. *Icarus* **1980**, *44*, 502–510. [CrossRef]
32. Becker, H.N.; Florence, M.M.; Brennan, M.J.; Hansen, C.J.; Schenk, P.M.; Ravine, M.A.; Arballo, J.K.; Bolton, S.J.; Lunine, J.I.; Guillaume, A.; et al. Surface features of Ganymede revealed in Jupiter-shine by Juno's Stellar Reference Unit. *Geophys. Res. Lett.* **2022**, *49*, e2022GL099139. [CrossRef]
33. Howett, C.J.A.; Spencer, J.R.; Pearl, J.; Segura, M. Thermal inertia and bolometric bond albedo values for Mimas, Enceladus, Tethys, Dione, Rhea and Iapetus as derived from Cassini/CIRS measurements. *Icarus* **2010**, *206*, 573–593. [CrossRef]
34. Filacchione, G.; D'Aversa, E.; Capaccioni, F.; Clark, R.N.; Cruikshank, D.P.; Ciarniello, M.; Cerroni, P.; Bellucci, G.; Brown, R.H.; Buratti, B.J.; et al. Saturn's icy satellites investigated by Cassini-VIMS. IV. Daytime temperature maps. *Icarus* **2016**, *271*, 292–313. [CrossRef]
35. Tyler, G.L.; Eshleman, V.R.; Anderson, J.D.; Levy, G.S.; Lindal, G.F.; Wood, G.E.; Croft, T.A. Radio science with Voyager 2 at Saturn: Atmosphere and ionosphere and the masses of Mimas, Tethys, and Iapetus. *Science* **1982**, *215*, 553–558. [CrossRef]
36. Tajeddine, R.; Rambaux, N.; Lainey, V.; Charnoz, S.; Richard, A.; Rivoldini, A.; Noyelles, B. Constraints on Mimas' interior from Cassini ISS libration measurements. *Science* **2014**, *346*, 322–324. [CrossRef]
37. Noyelles, B. Interpreting the librations of a synchronous satellite–How their phase assesses Mimas' global ocean. *Icarus* **2017**, *282*, 276–289. [CrossRef]
38. Neveu, M.; Rhoden, A.R. The origin and evolution of a differentiated Mimas. *Icarus* **2017**, *296*, 183–196. [CrossRef]
39. Rhoden, A.R.; Henning, W.; Hurford, T.A.; Patthoff, D.A.; Tajeddine, R. The implications of tides on the Mimas ocean hypothesis. *J. Geophys. Res. Planets* **2017**, *122*, 400–410. [CrossRef]
40. Rhoden, A.R.; Walker, M.E. The case for an ocean-bearing Mimas from tidal heating analysis. *Icarus* **2022**, *376*, 114872. [CrossRef]
41. Denton, C.A.; Rhoden, A.R. Tracking the evolution of an ocean within Mimas using the Herschel impact basin. *Geophys. Res. Lett.* **2022**, *49*, e2022GL100516. [CrossRef]
42. Rhoden, A.R. Mimas: Frozen Fragment, Ring Relic, or Emerging Ocean World? *Annu. Rev. Earth Planet. Sci.* **2023**, *51*, 367–387. [CrossRef]
43. Spencer, J.R.; Nimmo, F. Enceladus: An active ice world in the Saturn system. *Annu. Rev. Earth Planet. Sci.* **2013**, *41*, 693–717. [CrossRef]
44. Dougherty, M.K.; Khurana, K.K.; Neubauer, F.M.; Russell, C.T.; Saur, J.; Leisner, J.S.; Burton, M.E. Identification of a dynamic atmosphere at Enceladus with the Cassini magnetometer. *Science* **2006**, *311*, 1406–1409. [CrossRef]
45. Clark, R.N.; Curchin, J.M.; Jaumann, R.; Cruikshank, D.P.; Brown, R.H.; Hoefen, T.M.; Stephan, K.; Moore, J.M.; Buratti, B.J.; Baines, K.H.; et al. Compositional mapping of Saturn's satellite Dione with Cassini VIMS and implications of dark material in the Saturn system. *Icarus* **2008**, *193*, 372–386. [CrossRef]
46. Howett, C.J.A.; Spencer, J.R.; Hurford, T.; Verbiscer, A.; Segura, M. Thermophysical property variations across Dione and Rhea. *Icarus* **2014**, *241*, 239–247. [CrossRef]
47. Jennings, D.E.; Tokano, T.; Cottini, V.; Nixon, C.A.; Achterberg, R.K.; Flasar, F.M.; Kunde, V.G.; Romani, P.N.; Samuelson, R.E.; Segura, M.E.; et al. Titan surface temperatures during the Cassini mission. *Astrophys. J. Lett.* **2019**, *877*, L8. [CrossRef]
48. Niemann, H.B.; Atreya, S.K.; Bauer, S.J.; Carignan, G.R.; Demick, J.E.; Frost, R.L.; Gautier, D.; Haberman, J.A.; Harpold, D.N.; Hunten, D.M.; et al. The abundances of constituents of Titan's atmosphere from the GCMS instrument on the Huygens probe. *Nature* **2005**, *438*, 779–784. [CrossRef]
49. Schmedemann, N.; Neukum, G. Impact crater size-frequency distribution (SFD) and surface ages on Mimas. In Proceedings of the 42nd Annual Lunar and Planetary Science Conference, No. 1608, The Woodlands, TX, USA, 7–11 March 2011; p. 2772. Available online: https://www.lpi.usra.edu/meetings/lpsc2011/pdf/2772.pdf (accessed on 17 November 2023).
50. Multhaup, K.; Spohn, T. Stagnant lid convection in the mid-sized icy satellites of Saturn. *Icarus* **2007**, *186*, 420–435. [CrossRef]
51. Stooke, P.J. Geology of Mimas. Abstracts of the Lunar and Planetary Science Conference. In Proceedings of the Lunar and Planetary Science Conference, NASA Johnson Space Center, The Woodlands, TX, USA, 13–17 March 1989; Volume 20, p. 1069. Available online: https://adsabs.harvard.edu/full/1989LPI....20.1069S (accessed on 29 August 2023).

52. Croft, S.K. Mimas: Tectonic Structure and Geologic History. In *Reports of Planetary Geology and Geophysics Program, 1990*; NASA: Washington, DC, USA, 1991. Available online: https://ntrs.nasa.gov/api/citations/19920001546/downloads/19920001546.pdf (accessed on 11 March 2023).
53. Pike, R.J. Formation of complex impact craters: Evidence from Mars and other planets. *Icarus* **1980**, *43*, 1–19. [CrossRef]
54. Croft, S.K. The scaling of complex craters. *J. Geophys. Res. Solid. Earth* **1985**, *90*, C828–C842. [CrossRef]
55. Melosh, J.H.; Ivanov, B.A. Impact crater collapse. *Annu. Rev. Earth Planet. Sci.* **1999**, *27*, 385–415. [CrossRef]
56. Pierazzo, E.; Melosh, H.J. Understanding Oblique Impacts from Experiments, Observations, and Modeling. *Annu. Rev. Earth Planet. Sci.* **2000**, *28*, 141–167. [CrossRef]
57. Poelchau, M.H.; Kenkmann, T. Asymmetric signatures in simple craters as an indicator for an oblique impact direction. *Meteorit. Planet. Sci.* **2008**, *43*, 2059–2072. [CrossRef]
58. Elbeshausen, D.; Wünnemann, K.; Collins, G.S. The transition from circular to elliptical impact craters. *J. Geophys. Res. Planets* **2013**, *118*, 2295–2309. [CrossRef]
59. Krohn, K.; Jaumann, R.; Elbeshausen, D.; Kneissl, T.; Schmedemann, N.; Wagner, R.; Voigt, J.; Otto, K.; Matz, K.D.; Preusker, F.; et al. Asymmetric craters on Vesta: Impact on sloping surfaces. *Planet. Space Sci.* **2014**, *103*, 36–56. [CrossRef]
60. Bérczi, S. Eroded Crater. In *Encyclopedia of Planetary Landforms*; Springer: New York, NY, USA, 2014. [CrossRef]
61. Beddingfield, C.B.; Burr, D.M.; Tran, L.T. Polygonal impact craters on Dione: Evidence for tectonic structures outside the wispy terrain. *Icarus* **2016**, *274*, 163–194. [CrossRef]
62. Wagner, R.J.; Neukum, G.; Schmedemann, N.; Hartmann, O.; Wolf, U. September. Crater chains, double and multiple craters on the satellites of Saturn: Morphology and stratigraphy. In Proceedings of the European Planetary Science Congress, Rome, Italy, 19–24 September 2010; p. 676. Available online: https://meetingorganizer.copernicus.org/EPSC2010/EPSC2010-676-1.pdf (accessed on 17 November 2023).
63. Hargitai, H. Chasma, Chasmata. In *Encyclopedia of Planetary Landforms*; Springer: New York, NY, USA, 2014. [CrossRef]
64. Bradák, B.; Nishikawa, M.; Gomez, C. A Theory about a Hidden Evander-Size Impact and the Renewal of the Intermediate Cratered Terrain on Dione. *Universe* **2023**, *9*, 247. [CrossRef]
65. Öhman, T.; Aittola, M.; Korteniemi, J.; Kostama, V.P.; Raitala, J. Polygonal impact craters in the solar system: Observations and implications. *Geol. Soc. Am. Spec. Pap.* **2010**, *465*, 51–65. [CrossRef]
66. Beddingfield, C.B.; Cartwright, R.J. Hidden tectonism on Miranda's Elsinore Corona revealed by polygonal impact craters. *Icarus* **2020**, *343*, 113687. [CrossRef]
67. Bradák, B.; Kimura, J.; Asahina, D.; El Yazidi, M.; Orgel, C. Introduction to Dione's Wispy Terrain as a Putative Model Region for "Micro" Wilson Cycles on Icy Satellites. *Remote Sens.* **2023**, *15*, 5177. [CrossRef]
68. Sekiguchi, N. On the fissions of a solid body under the influence of tidal force; with application to the problem of twin craters on the Moon. *Moon* **1970**, *1*, 429–439. [CrossRef]
69. Zahnle, K.J.; Alvarellos, J.L.; Dobrovolskis, A.R.; Hamill, P. Secondary and sesquinary impact craters on Europa. *Icarus* **2008**, *194*, 660–674. [CrossRef]
70. Bruesch, L.S.; Asphaug, E. Modeling global impact effects on middle-sized icy bodies: Applications to Saturn's moons. *Icarus* **2004**, *168*, 457–466. [CrossRef]
71. Moore, J.M.; Schenk, P.M.; Bruesch, L.S.; Asphaug, E.; McKinnon, W.B. Large impact features on middle-sized icy satellites. *Icarus* **2004**, *171*, 421–443. [CrossRef]
72. Moore, J.M.; Ahern, J.L. The geology of Tethys. *J. Geophys. Res. Solid. Earth* **1983**, *88*, A577–A584. [CrossRef]
73. Schenk, P.M. Crater formation and modification on the icy satellites of Uranus and Saturn: Depth/diameter and central peak occurrence. *J. Geophys. Res. Solid. Earth* **1989**, *94*, 3813–3832. [CrossRef]
74. Prockter, L.M.; Patterson, W. Morphology and evolution of Europa's ridges and bands. In *Europa*; Pappalardo, R.T., McKinnon, W.B., Khurana, K.K., Eds.; University of Arizona Press: Tucson, AZ, USA, 2009; pp. 237–258. [CrossRef]
75. Dameron, A.C.; Burr, D.M. Europan double ridge morphometry as a test of formation models. *Icarus* **2018**, *305*, 225–249. [CrossRef]
76. Quillen, A.C.; Giannella, D.; Shaw, J.G.; Ebinger, C. Crustal failure on icy moons from a strong tidal encounter. *Icarus* **2016**, *275*, 267–280. [CrossRef]
77. Matsuyama, I.; Beuthe, M.; Hay, H.C.; Nimmo, F.; Kamata, S. Ocean tidal heating in icy satellites with solid shells. *Icarus* **2018**, *312*, 208–230. [CrossRef]
78. Hay, H.C.; Matsuyama, I. Nonlinear tidal dissipation in the subsurface oceans of Enceladus and other icy satellites. *Icarus* **2019**, *319*, 68–85. [CrossRef]